Genetics inMedicine

www.nature.com/gim

Check for updates

ARTICLE

Disrupted intraflagellar transport due to *IFT74* variants causes Joubert syndrome

Minna Luo[1,9], Zaisheng Lin[2,9], Tian Zhu[3,9], Minjun Jin[4,9], Dan Meng[5], Ruida He[2], Zongfu Cao[1], Yue Shen[1], Chao Lu[1], Ruikun Cai[1], Yong Zhao[6], Xueyan Wang[7], Hui Li[3], Shijing Wu[3], Xuan Zou[3], Guanjun Luo[6], Li Cao[8], Min Huang[2], Huike Jiao[2], Huafang Gao[1], Ruifang Sui[3]✉, Chengtian Zhao[4]✉, Xu Ma[1]✉ and Muqing Cao[2]✉

PURPOSE: Ciliopathies are a group of disorders caused by defects of the cilia. Joubert syndrome (JBTS) is a recessive and pleiotropic ciliopathy that causes cerebellar vermis hypoplasia and psychomotor delay. Although the intraflagellar transport (IFT) complex serves as a key module to maintain the ciliary structure and regulate ciliary signaling, the function of IFT in JBTS remains largely unknown. We aimed to explore the impact of IFT dysfunction in JBTS.

METHODS: Exome sequencing was performed to screen for pathogenic variants in IFT genes in a JBTS cohort. Animal model and patient-derived fibroblasts were used to evaluate the pathogenic effects of the variants.

RESULTS: We identified *IFT74* as a JBTS-associated gene in three unrelated families. All the affected individuals carried truncated variants and shared one missense variant (p.Q179E) found only in East Asians. The expression of the human p.Q179E-IFT74 variant displayed compromised rescue effects in zebrafish *ift74* morphants. Attenuated ciliogenesis; altered distribution of IFT proteins and ciliary membrane proteins, including ARL13B, INPP5E, and GPR161; and disrupted hedgehog signaling were observed in patient fibroblasts with *IFT74* variants.

CONCLUSION: *IFT74* is identified as a JBTS-related gene. Cellular and biochemical mechanisms are also provided.

Genetics in Medicine (2021) 23:1041–1049; https://doi.org/10.1038/s41436-021-01106-z

INTRODUCTION

The primary cilium is an antenna-like cellular organelle that protrudes from the cell surface and serves as a versatile platform for environmental sensing and signaling coordination.[1,2] Originating from the basal body, the primary cilium is assembled by intraflagellar transport (IFT), an evolutionarily conserved kinesin- and dynein-driven bidirectional trafficking system composed of two subcomplexes, IFT-A and IFT-B, organized from approximately 20 proteins.[3,4] Ciliary defects cause a number of human diseases, collectively known as ciliopathies, which affect several major organs and show a plethora of highly variable clinical features and divergent phenotypic severities.[1–3,5] Joubert syndrome (JBTS, OMIM 213300) is a recessive and heterogeneous ciliopathy that mainly affects the brain, and is characterized by the malformation of the cerebellar vermis and brain stem, which is recognized as the molar tooth sign (MTS) by brain magnetic resonance imaging (MRI).[6] The clinical features of JBTS include developmental delay, hypotonia, a dysregulated breathing pattern, and/or abnormal ocular movement.[7–9]

To date, all known JBTS-related genes encoding proteins localize around cilia, and dysfunctions of these proteins alter ciliary compositions or signaling.[10–13] Interestingly, the relationship between JBTS and the IFT complex, a major module regulating ciliary composition by transporting components inside the cilia,[4] remains largely unknown; thus far, only two siblings with Jeune asphyxiating thoracic dystrophy (JATD, OMIM 208500)/Mainzer–Saldino syndrome (MZSDS, OMIM 266920) harboring *IFT172* variants accompanied with cerebellar vermis hypoplasia have been identified.[14]

To explore the roles of IFT in JBTS, we performed exome sequencing in a Chinese JBTS cohort and identified *IFT74* as a JBTS-related gene. Surprisingly, all the patients shared a variant found only in East Asians and we confirmed the pathogenicity of the variant in a zebrafish model. We found that variants in *IFT74* disrupted the IFT complex, impaired the ciliary localization of ARL13B and INPP5E, and altered ciliary-related signaling.

MATERIALS AND METHODS

See Supplementary Materials for detailed methods.

RESULTS

Identification of *IFT74* recessive variants by exome sequencing in a Chinese cohort with JBTS

We enrolled a Chinese cohort of 151 affected individuals with a diagnosis of JBTS and we mainly focused on IFT genes and other known ciliopathy genes (Table S1). A number of rare deleterious variants at the *IFT* locus were observed by exome sequencing, most of which were heterozygous in one allele and could not

[1]National Human Genetic Resources Center, National Research Institute for Family Planning, Beijing, China. [2]Key Laboratory of Cell Differentiation and Apoptosis of Chinese Ministry of Education, Department of Pathophysiology, Shanghai Jiao Tong University School of Medicine, Shanghai, China. [3]Department of Ophthalmology, Peking Union Medical College Hospital, Peking Union Medical College, Chinese Academy of Medical Sciences, Beijing, China. [4]Institute of Evolution and Marine Biodiversity, Ocean University of China, Qingdao, China. [5]Tianjin Key Laboratory of Food and Biotechnology, School of Biotechnology and Food Science, Tianjin University of Commerce, Tianjin, China. [6]Child Rehabilitation Department, Nanhai Affiliated Maternity and Children's Hospital of Guangzhou University of TCM, Foshan, China. [7]Department of Prenatal Diagnosis, The Affiliated Women's and Children's Hospital of Chengdu Medical College, Chengdu, China. [8]Child Healthcare Department, The Affiliated Women's and Children's Hospital of Chengdu Medical College, Chengdu, China. [9]These authors contributed equally: Minna Luo, Zaisheng Lin, Tian Zhu, Minjun Jin. ✉email: hrfsui@163.com; chengtian_zhao@ouc.edu.cn; maxu_nhgrc@163.com; muqingcao@sjtu.edu.cn

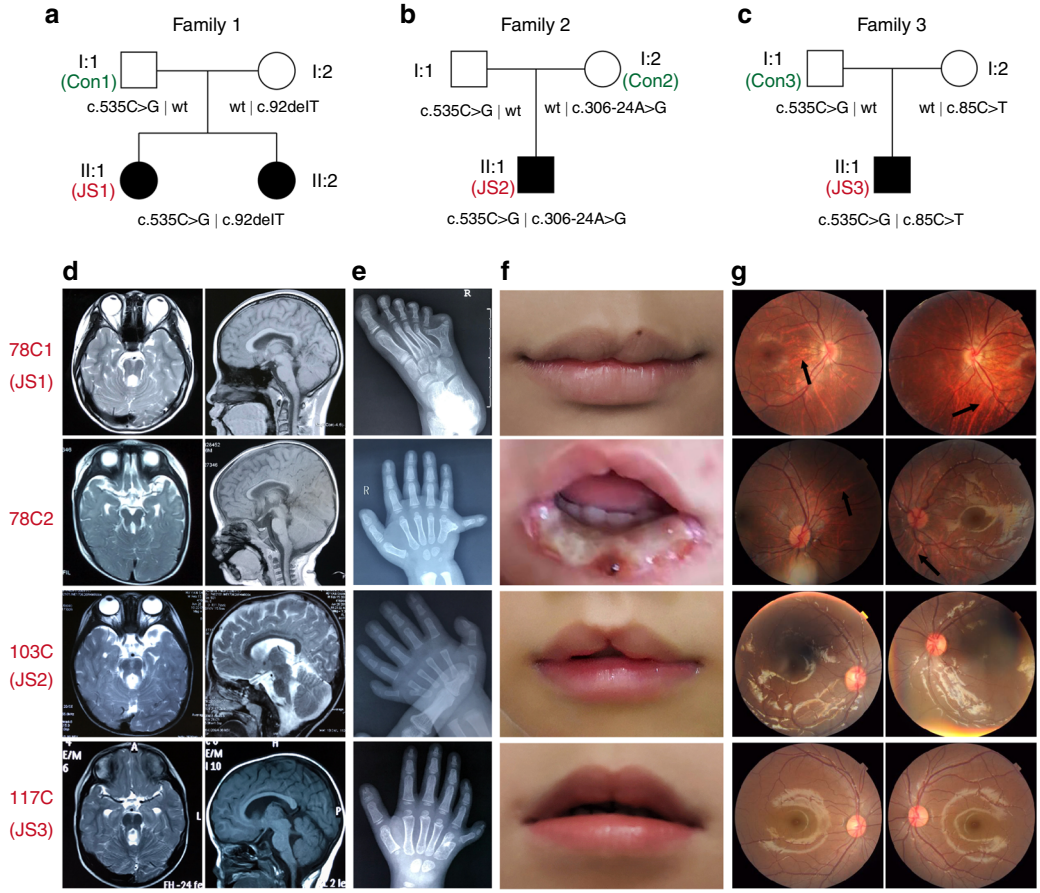

Fig. 1 Clinical features of individuals with variants in *IFT74*. (**a**–**c**) Pedigrees of Joubert syndrome (JBTS) families with *IFT74* variants. (**d**) Representative brain magnetic resonance images (MRIs) for affected individuals 78C1, 78C2, 103C, and 117C, showing the molar tooth sign (MTS). (**e**) Images showing postaxial polydactyly in the affected individuals. (**f**) Facial photos of patients 78C1, 78C2, 103C, and 117C showing minor midline notches in the upper lips. The cleft lip in 78C1 had been surgically repaired. (**g**) Fundus appearance of the affected individuals. Small optic discs and nasal retinal nerve fiber layer (RNFL) thinning with the emerged choriocapillaris (black arrow) in patients 78C1 and 78C2. The fundus appeared normal in patients 103C and 117C.

explain the cause of JBTS (Table S2). Surprisingly, four affected individuals from three unrelated families were identified as having biallelic variants in *IFT74* (NM_025103.2), which encodes a subunit of the IFT-B core complex. The IFT74/81 heterodimer nucleates with IFT22 and the IFT25/27 dimer to form the IFT-B inner core, which interacts with IFT46, IFT52, IFT56, IFT70, and IFT88 to form the IFT-B core complex. The index cases were found in a family (family 1), while no biallelic variants in known JBTS genes were revealed (Fig. 1a, Table S3). The biallelic variants of *IFT74* were c.92delT (p.L31Hfs*25) and c.535C>G (p.Q179E) (Fig. S1a), which were confirmed to be segregated in an autosomal recessive mode of inheritance (Fig. 1a). The maternally inherited frameshift variant, c.92delT in exon 1, was a novel variant and has not been found in the public databases dbSNP, ExAC, or gnomAD, or in our in-house variant repository. This variant was classified as pathogenic according to the American College of Medical Genetics and Genomics (ACMG) guidelines.[15] The paternally inherited missense variant, c.535C>G, was annotated as rs150219690 in the dbSNP database. It was rare in the gnomAD database, found in 19 of 221,326 alleles with a frequency of 0.00008585. Interestingly, all 19 heterozygous alleles were detected in East Asians (allele frequency 0.001406).[16] The substitution at residue 179 was predicted to be benign, tolerated, and disease-causing by PolyPhen-2, SIFT and MutationTaster, respectively. Thus, this variant was annotated as a variant of uncertain significance (VUS).

Two additional individuals, patient 103C and patient 117C, with *IFT74* variants were then identified in this Chinese JBTS cohort (Fig. 1b, c, Fig. S1b, c, Table S3). These two patients harbored the same paternally inherited heterozygous variant (c.535C>G, p.Q179E) but had different maternally inherited variants in *IFT74*: c.306-24A>G in family 2 and c.85C>T (p.R29*) in family 3 (Fig. 1b, c, Fig. S1b, c). The intronic variant c.306-24A>G was predicted to be a branch site of splicing and was conserved in several species. Reverse transcription polymerase chain reaction (RT-PCR) results showed the skipping of exon 5 in *IFT74* caused by c.306-24A>G, which resulted in a 33–amino acid in-frame deletion in IFT74 in patient 103C and his mother (Fig. S2a–c). The stop-gained variant c.85C>T (p.R29*) in family 3 was predicted to cause early truncation. Therefore, the c.306-24A>G and c.85C>T (p.R29*) variants were classified as likely pathogenic and pathogenic, respectively.

The four affected individuals were from three nonconsanguineous families. None of the parents had a positive personal or familial medical history. All patients presented with MTS on brain MRI, delay in global developmental milestones, postaxial polydactyly, and subtle cleft of the upper lip (Fig. 1d–f, Table 1). Fundus photographs showed small optic discs in both eyes, and optical coherence tomography (OCT) images demonstrated nasal retinal nerve fiber layer (RNFL) thinning in the siblings in family 1 (Fig. 1g), suggesting the feature of optic nerve hypoplasia in

Table 1. Clinical features of JBTS and BBS patients with biallelic *IFT74* variants.

Patient ID	78C1 (Family 1_II:1)	78C2 (Family 1_II:2)	103C (Family 2_II:1)	117C (Family 3_II:1)	*IFT74*-BBS case 1 (Lindstrand)	*IFT74*-BBS case 2 (Kleinendorst)
Age	13 years 5 months	1 year 11 months	4 years 6 months	7 years 2 months	36 years	11 years
Gender	Female	Female	Male	Male	Male	Female
Ethnicity	Chinese	Chinese	Chinese	Chinese	NA	Dutch
Variant 1	c.92delT (p.L31Hfs*25)	c.92delT (p.L31Hfs*25)	c.306-24A>G (p.103_135del)	c.85C>T (p.R29*)	Deletion of exon 14–19	c.371_372del (p.Q124Rfs*9)
Variant 2	c.535C>G (p.Q179E)	c.535C>G (p.Q179E)	c.535C>G (p.Q179E)	c.535C>G (p.Q179E)	c.1685-1G>T	c.1685-1G>T
Height (cm)	148.5	78	104	116	NA	162.7
Weight (kg)	40	8.9	14	17.8	NA	70.94
BMI (kg/m^2)	18.14	14.63	12.94	13.23	NA	26.80
Molar tooth sign	+	+	+	+	−	−
Oculomotor apraxia	−	+	+	+	NA	−
Respiratory abnormality	−	+	+	−	NA	−
Hypotonia	+	+	+	+	NA	−
Retinal involvement	−	−	−	−	Retinitis pigmentosa	Rod–cone dystrophy
Optic nerve hypoplasia/ RNFL defect	+/+	+/+	−/−	−/+	NA/NA	−/−
Renal involvement	−	−	−	−	−	−
Liver involvement	−	−	−	−	NA	−
Postaxial polydactyly	+	+	+	+	+	+
Developmental delay	+	+	+	+	−	−[a]
Intellectual disability	−	Moderate	Mild	Mild	+	−
Hypogonadism (in males) or genital abnormalities (in females)	−	−	−	−	Hypogonadism	−
Craniofacial dysmorphisms	Midline cleft lip	Midline notch in the upper lip	Midline cleft lip	Midline notch in the upper lip	Microcephaly	Macrocephaly[b]
Truncal obesity	−	−	−	−	+	+
Diabetes mellitus	−	−	−	−	−	−
Behavioral problem	−	Self-mutilation	−	−	−	−

BBS Bardet–Biedl syndrome, *BMI* body mass index, *JBTS* Joubert syndrome, *NA* not available or not mentioned, *RNFL* retinal nerve fiber layer, − not present, + present.
[a]Only speech delay in childhood.
[b]Her father has an occipitofrontal circumference of +2 SD.

patients 78C1 and 78C2, which was an ophthalmological feature not previously described in other JBTS patients.[6,17] Pattern electroretinogram (PERG) and pattern visual evoked potential (PVEP) confirmed the presence of ocular defects in patient 78C1 but the absence in patients 103C and 117C, though the test was not performed due to the young age of patient 78C2 (Fig. S3a–c). Renal/hepatic involvement, obesity, or hypogonadism/genital abnormalities were not detected in any of these patients (Table 1). More detailed information on each patient is provided in the supplemental clinical reports (Supplementary materials). The combination of the clinical features, MTS, polydactyly, and midline cleft/notch of the upper lip indicates that these patients belong to the oral–facial–digital subtype of JBTS. To the best of our knowledge, the combination of the oral–facial–digital subtype with optic nerve hypoplasia in 78C1 and 78C2 may represent an unreported subgroup of JBTS.

The p.Q179E variant disrupts the functions of IFT74

IFT74 is a highly conserved protein that forms a heterodimer with IFT81 to nucleate the IFT-B subcomplex.[18–20] Previous studies showed that variants in *IFT74* (BBS20, OMIM 608040) were associated with Bardet–Biedl syndrome (BBS, OMIM 209900). In contrast to the cerebellar and brain stem malformation features of JBTS, BBS is another ciliopathy characterized by polydactyly,

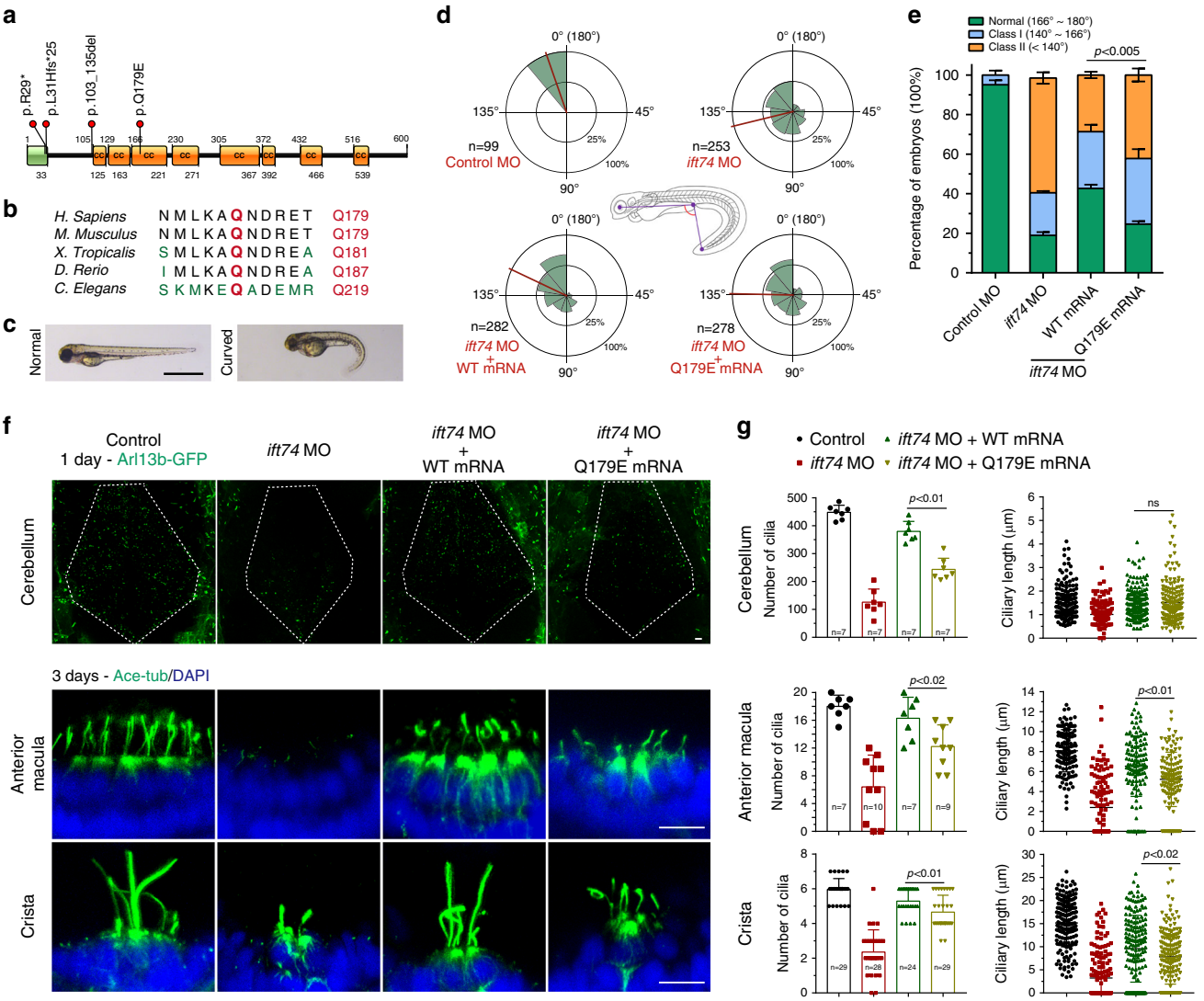

Fig. 2 Loss of *ift74* in zebrafish leads to ciliopathy phenotypes, and IFT74 p.Q179E messenger RNA (mRNA) fails to rescue the phenotypes. (**a**) Schematic representation of IFT74 and locations of variants identified in this study. CC coiled-coil domain. (**b**) Alignment of diverse IFT74 sequences reveals that glutamine at the position corresponding to Q179 of the human sequence (red) is evolutionarily conserved. (**c**) Phenotypes of the embryos of zebrafish injected with morpholino (MO) oligonucleotides. Scale bar, 0.5 mm. (**d**,**e**) Statistical results showing the distribution of body curvature angles in each group as indicated. The angles were measured by drawing two lines between the center of the eye, cloaca, and tip of the tail. The red line in each coxcomb chart represents the average mean of the curvature angles (**d**). The Control MO or *ift74* MO were also coinjected with green fluorescent protein (GFP) mRNA. The embryos were grouped into three categories according to their body curvature severity. Normal (166°–180°), class I (140°–166°), and class II (<140°). (**f**) Representative confocal images showing cilia (green) in the cerebellum (indicated by white dotted lines), ear macula, and crista in different groups of embryos as indicated. Cilia in the cerebellum were visualized using the *Tg (β-actin:Arl13b-GFP)* transgenic line at 1 day post fertilization. Cilia in the ear maculae and cristae were immunostained with anti-acetylated tubulin (Ace-tub) antibody on zebrafish larvae at 3 days post fertilization. Nuclei were counterstained with DAPI in blue. Scale bars, 10 μm. (**g**) Quantification of the number and length of cilia in cerebellum, ear macula, and crista. Error bars represent the standard deviation (SD) in (**e**) and (**g**). Statistical significance was determined using the χ^2 test in (**e**) and the *t*-test in (**g**).

retinal degeneration, obesity, intellectual disability, renal dysfunction, and hypogonadism (Table 1).[21,22] Both of the reported BBS cases carried a truncated allele (deletion of exons 14–19 in case 1 and a frameshift variant p.Q124Rfs*9 in case 2) and shared another variant (c.1685-1G>T), which might affect splicing, therefore resulting in a change of the last 40 amino acids (561–600) at the C-terminus of the IFT74 protein.[21,22] In our study, none of the affected individuals presented with typical features of BBS, such as obesity or hypogonadism/genital abnormalities (Table 1). Interestingly, except for one truncated allele, all four individuals shared the c.535C>G (p.Q179E) variant (Fig. 2a), and haplotype analysis suggested a founder effect of this recurrent variant (Table S4). The alignment of IFT74 sequences from multiple ciliated organisms shows that the residues at the position corresponding to human glutamine 179 are highly conserved, suggesting that the residue is functionally important (Fig. 2b). We first tested the pathogenicity of this IFT74 variant in zebrafish. Knockdown of the *ift74* gene resulted in severe ventral body curvature, a characteristic phenotype of cilia mutants (Fig. 2c–e).[23] To quantify the body curvature phenotype, we measured the angles between the head and tail (Fig. 2d) and plotted the distribution of angles (Fig. 2d). We grouped the *ift74* morphants into three categories according to their body curvature severity (Fig. 2e). The injection of *ift74* morpholino (MO) produced a large number of class I and class II

embryos (Fig. 2d, e). Overexpression of human *IFT74* gene significantly suppressed body curvature defects in these morphants. Noticeably, the rescue efficiency of the human p.Q179E variant was significantly lower than that of wild-type IFT74 (Fig. 2d, e, Fig. S4a–d). Further analysis suggested that knockdown of *ift74* resulted in defects in ciliogenesis in the cerebellum (Fig. 2f, g) as well as in other tissues (Fig. 2f, g, Fig. S4e). Consistently, the human p.Q179E variant also showed compromised rescue efficiency compared with wild-type IFT74 (Fig. 2f, g, Fig. S4e). These results demonstrate that glutamine 179, a highly conserved residue, is important for the physiological function of IFT74.

Aberrant cilia biogenesis in JBTS patient fibroblasts with *IFT74* variants

To assess the potential effects of *IFT74* variants on the primary cilia, we set out to generate fibroblast cell lines from skin biopsy specimens obtained from three *IFT74*-JBTS patients (78C1, 103C, 117C), their parents, and one healthy individual (Fig. 1a–c). We first examined cilia of mutant versus wild-type cells 48 hours after serum starvation. Immunocytochemistry for CEP164 and acetylated tubulin showed similar ciliation in patient and control fibroblasts (Fig. 3a, b). Ciliary length was variable in all patient and control fibroblasts, whereas the ciliary length of patient cells was distributed over a much broader range (Fig. 3a–c). Furthermore, an appreciable difference was observed in the length of the cilia, with three patient cells having significantly longer cilia than three control cells (3.4 vs. 5.5 µm, 3.7 vs. 4.4 µm, and 3.6 vs. 5.0 µm) (Fig. 3c). Finally, we assessed the early stages of ciliogenesis after 5 and 12 hours of serum starvation. The ciliation of patient cells after 5 hours of serum starvation was significantly less than that of control cells, suggesting the occurrence of compromised early-stage ciliogenesis in patient cells (Fig. 3d). Taken together, these results indicate that *IFT74* variants lead to abnormal ciliogenesis in patient fibroblasts.

Reduced IFT74 and IFT81 proteins in patient fibroblasts with *IFT74* variants

To determine the potential effects of the variants in *IFT74*, we assessed the protein levels in patient and control fibroblasts by immunoblot assay. No obvious difference in IFT74 protein level was observed between the three parents (with one mutated allele and one wild-type allele) and the healthy control (with two wild-type *IFT74* alleles) (Fig. 3e, f). This result demonstrates that one wild-type *IFT74* allele is sufficient to maintain normal IFT74 protein levels in fibroblast cells. In all three mutated cell lines with a nonsense/truncated allele and the c.535C>G variant (p.Q179E), full-length IFT74 proteins were largely reduced compared with the control cells (Fig. 3e, f), and the protein products of the c.306-24A>G variant were reduced in Con2 and JS2 as well (Fig. 3e). To investigate whether the p.Q179E variant caused the instability of IFT74, we examined IFT74 turnover in control and patient cells with cycloheximide treatment to inhibit new protein synthesis. Faster degradation of the mutated IFT74 protein was observed by immunoblot analysis (Fig. S5a, b). Since it has been reported that the complete loss of *IFT74* in *Chlamydomonas* destabilizes both core and peripheral proteins of the IFT-B complex,[20,24] we assessed the protein levels of IFT proteins in control and patient fibroblasts. Interestingly, we found that only IFT81, but not IFT88, was reduced in patient cells (Fig. 3e). Consistent with the results found in *Chlamydomonas*,[20] IFT-A protein IFT140 was not reduced in patient cells (Fig. 3e). IFT74 and IFT81 form a heterodimer that is the inner core of the IFT-B core complex, and altered integrity of the complex may affect the stabilities of the subunits. We carried out coimmunoprecipitation (Co-IP) experiments, and we found that the interactions of IFT81 with wild-type or p.Q179E-mutated IFT74 were not changed (Fig. S5c), indicating that the loss of IFT81 in patient fibroblasts was not caused by alteration in protein interactions. To determine whether the loss of IFT81 was caused by the instability of IFT74, we knocked down IFT74 in RPE1 cells by small interfering RNA (siRNA), and IFT81 levels were reduced significantly (Fig. 3g). Furthermore, the overexpression of either wild-type or Q179E IFT74 restored IFT81 protein levels in IFT74 siRNA-transfected cells (Fig. 3g). These results indicate that the downregulation of IFT81 in patient cells is mainly caused by the instability of mutated IFT74.

The interaction of p.Q179E variant with IFT27 (BBS19) is comparable with wild-type IFT74

The IFT74/81 core interacts with the IFT25/27 dimer to regulate the transport of BBSome in cilia.[25] Co-IP showed that the interactions of IFT27 with wild-type IFT74 or p.Q179E IFT74 (JBTS variant) were similar, but Δ561–600-IFT74 (BBS variant) abolished its interaction with IFT27 (Fig. S5d). Considering the role of IFT27 in BBS, the phenotypes of the two *IFT74*-related BBS patients may be caused by the attenuated interaction of Δ561–600-IFT74 with IFT27 (Fig. S5e). This result provided a possible explanation regarding why the p.Q179E variant did not lead to BBS (Fig. S5e).

Dysregulation of the distribution of IFT components in the cilia of patient fibroblasts

To determine whether IFT was affected in the cilia, we examined IFT74, IFT88, and IFT140 in patient and control fibroblasts subjected to 48 hours of serum starvation to induce ciliogenesis. Immunostaining indicated that the two IFT-B components, IFT74 and IFT88, were less abundant in the patient fibroblasts than in the control fibroblasts (Fig. 3h, i, k, and l, Fig. S6a, b), whereas the IFT-A protein IFT140 accumulated in all patient cells (Fig. 3j, m, Fig. S6c). These results indicated that variants in IFT74 disrupted intraflagellar transport in cilia of patient cells.

Aberrant intraflagellar transport impairs ARL13B and INPP5E transport in cilia

To further investigate the intrinsic link between *IFT74* variants and JBTS, we examined the subcellular localization of a series of JBTS-related proteins in patient and control fibroblasts. Immunostaining showed that two transition zone proteins, TMEM67[26,27] and TCTN1,[10,27] and one centrosomal satellite protein, OFD1,[28] localized normally in patient and control fibroblasts (Fig. 3n–p). Interestingly, we noticed that the staining of ARL13B,[29,30] a ciliary membrane–associated small GTPase, in patient cells was slightly weaker than that in control cells, and it has been reported that the disruption of IFT led to a reduction of ARL13B in cilia, though the mechanism remains unclear.[30–32] We quantified the ciliary localization of ARL13B, and we found that ciliary ARL13B was slightly reduced in patient cells compared with control cells (Fig. 4a, c, Fig. S7a). Another JBTS-related protein, INPP5E, a phosphoinositide 5-phosphatase that dephosphorylates ciliary PI(4,5)P_2 to PI(4)P,[33,34] was significantly reduced in patient cilia (Fig. 4b, d, Fig. S7b). Thus, our results indicate that ciliary composition is aberrant in fibroblasts with *IFT74* variants.

IFT74 mutant cells displayed abnormal sonic hedgehog signaling

It is well established that cilia play a key role in the regulation of the hedgehog pathway,[35,36] and aberrant hedgehog signaling has been shown to be associated with JBTS.[37,38] The presence of polydactyly in patients with *IFT74* variants and the observation of reduced ARL13B and INPP5E levels in patient cilia prompted us to further assess the hedgehog pathway in patient fibroblasts. We monitored the expression of the hedgehog-responsive genes *GLI1* and *PTCH1*, which are upregulated during hedgehog activation. Although quantitative PCR showed that *GLI1* was upregulated in response to smoothened agonist (SAG) treatment in both control and patient fibroblasts, the response of patient cells was markedly

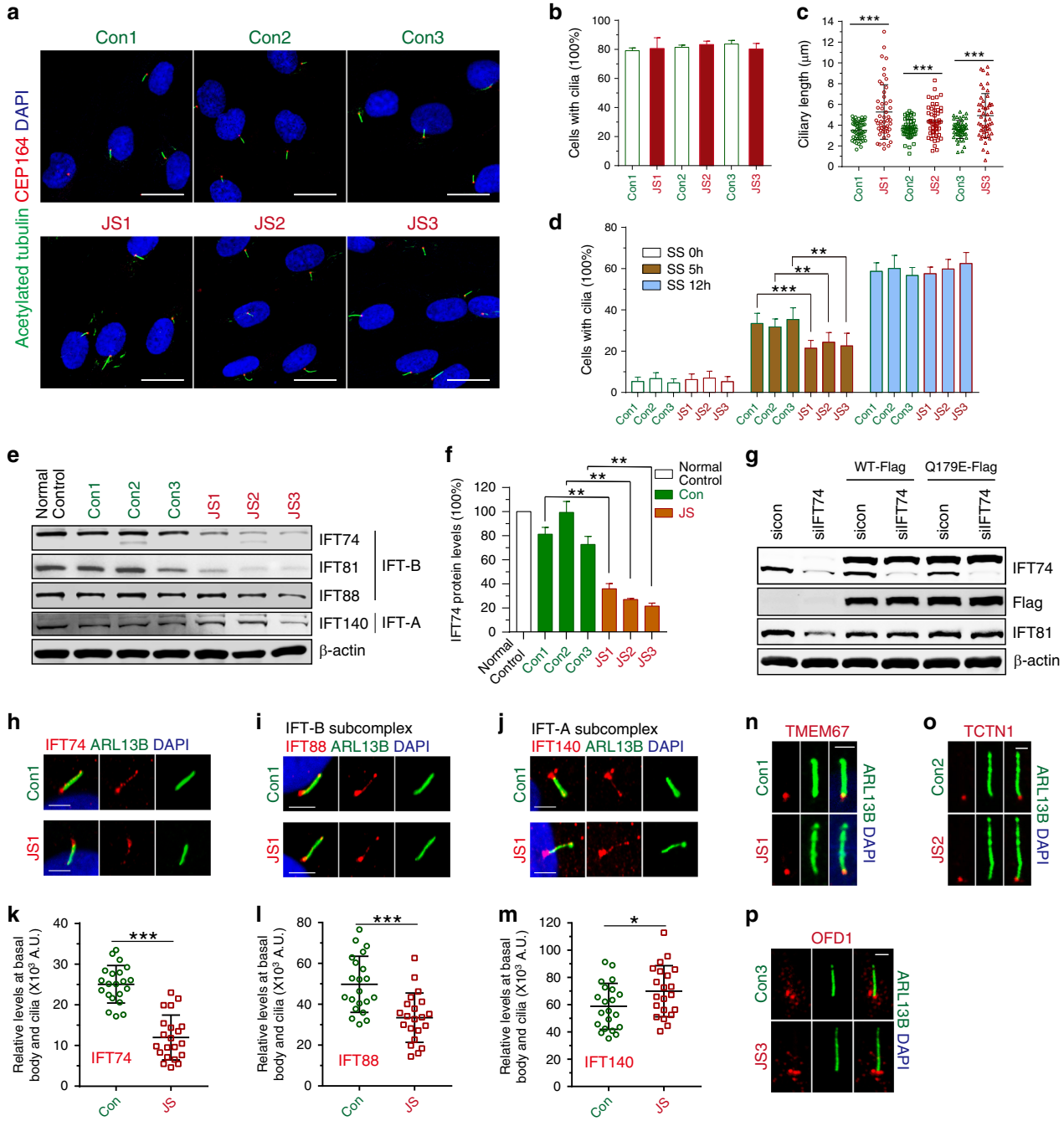

Fig. 3 ***IFT74*-related Joubert syndrome (JBTS) is associated with defects of cilia.** (**a**) Representative images of control and patient fibroblasts stained for acetylated tubulin (green), CEP164 (red), and DAPI (blue). Cells were treated with serum starvation for 48 hours before fixation. Scale bars, 30 μm. (**b**) Quantification of cells with cilia from healthy controls and JBTS patients. (**c**) Quantification of ciliary length of the fibroblasts. (**d**) Quantification of cells with cilia after the treatment of serum starvation for 0 hours, 5 hours, and 12 hours. (**e**) Western blots of whole cells probed with the indicated antibodies. (**f**) Quantification of IFT74 protein levels relative to the β-actin loading control. Statistical significance was determined by the *t*-test (**$p < 0.01$). (**g**) Western blots of protein levels of RPE1 cells by probing indicated antibodies. Wild-type cells or cells stably expressing wt-IFT74-Flag or Q179E-IFT74-Flag were transfected with control small interfering RNA (siRNA) or siRNA targeted *IFT74*. (**h**–**j**) Representative images of fibroblasts stained for IFT74, IFT88, or IFT140 and costained for ARL13B to indicate cilia. Scale bars, 3 μm. (**k**–**m**) Quantification of IFT protein levels (in **h**–**j**) in cilia. (**n**–**p**) Representative images of fibroblasts stained for TMEM67 (red) and ARL13B (green) (**n**), TCTN1 (red) and ARL13B (green) (**o**), OFD1 (red) and ARL13B (green) (**p**). Scale bars, 1.5 μm. Error bars represent SD.

attenuated (Fig. 4e). *PTCH1* showed a consistent pattern only in JS1 (Fig. 4f). However, *PTCH1* expression in the other two families was similar, and the variation in expression precluded reaching statistical significance (Fig. 4f). During the activation of the hedgehog pathway, SMO accumulates in cilia, while PTCH1 and GPR161 exit from cilia.[2,39] INPP5E dephosphorylates ciliary PI(4,5) P_2 to PI(4)P to promote the TULP3-dependent removal of GPR161 from cilia.[34,39,40] To further investigate why *IFT74* mutated fibroblasts showed impaired hedgehog sensitivity, we examined SMO and GPR161 in cilia by immunofluorescence. Interestingly, upon SAG treatment, SMO redistribution was similar in both patient and control fibroblasts (Fig. 4g, j). Upon SAG treatment,

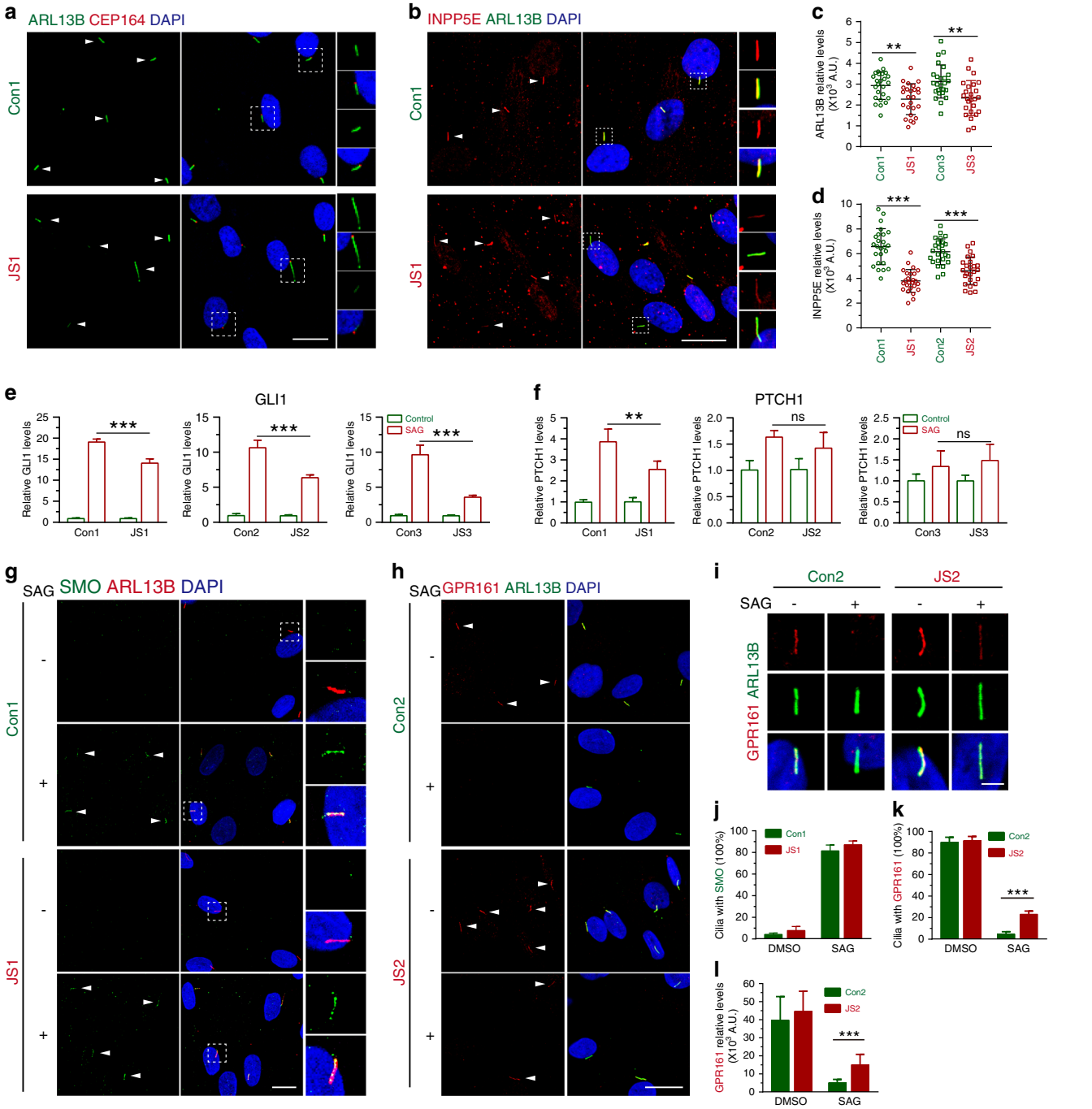

Fig. 4 Alteration of ciliary composition and cilia-related signaling in patient fibroblasts. (**a**,**b**) Representative immunofluorescence images of fibroblasts stained for CEP164 (red) and ARL13B (green) in (**a**); INPP5E (red) and ARL13B (green) in (**b**). The arrowheads indicate cilia. Scale bars, 20 μm. (**c**,**d**) Quantification of relative levels of ARL13B (**a** and Fig. S7a) and INPP5E (**b** and Fig. S7b) in cilia. Statistical significance was determined by the *t*-test (**$p < 0.01$). (**e**,**f**) Quantitative real-time polymerase chain reaction (PCR) analysis of *GLI1* (**e**) and *PTCH1* (**f**) expression in fibroblasts. The cells were subjected to serum starvation for 48 hours followed by SAG treatment or no SAG treatment for 24 hours. Three biological repeats were used for each group. Statistical significance was determined by the *t*-test (**$p < 0.01$; ***$p < 0.001$; ns not significant). (**g**–**i**) Representative immunofluorescence images of fibroblasts stained for SMO (green) and ARL13B (red) in (**g**); GPR161 (red) and ARL13B (green) in (**h**,**i**). The cells were subjected to serum starvation for 48 hours followed by SAG treatment or no treatment for 24 hours. Scale bars are 20 μm in (**g**,**h**) and 3 μm in (**i**). (**j**–**l**) Quantification of cilia positive for SMO (**g**) and GPR161 (**h**, **i**). Statistical significance was determined by the *t*-test (***$p < 0.001$). Error bars represent SD.

GPR161 was cleared from the cilia of control fibroblasts, while the levels of the protein in the patient cilia remained substantial (Fig. 4h, k). Furthermore, GPR161 labeling showed a higher ciliary intensity in patient fibroblasts than in control fibroblasts (Fig. 4i, l). Taken together, our results indicate that attenuated hedgehog signaling in patient fibroblasts is associated with aberrant accumulation of GPR161 in cilia. Moreover, reduced ciliary INPP5E (Fig. 4b, d) may account for the impaired removal of GPR161 from patient cilia. Thus, the data showed that variants in *IFT74* resulted in the disruption of cilia-related signaling.

DISCUSSION

In this study, we revealed the link between JBTS and the core IFT-B protein IFT74, and we identified four novel pathogenic variants of *IFT74*, in particular, an allele (c.535C>G) found only in East Asians. All four patients presented diagnostic MTS in brain MRI and other main JBTS-related clinical features, including developmental delay, neonatal hypotonia, and/or oculomotor apraxia. The patients shared two additional characteristic features, postaxial polydactyly, and subtle midline cleft/notch of the upper lip. Half of the patients (2/4) presented a distinct appearance of the fundus: small optic discs with sector RNFL thinning. These data suggest that optic nerve hypoplasia may be a characteristic phenotype that has not been mentioned in JBTS and is worthy of further investigation in more JBTS patients. None of the affected individuals had renal defects, obesity, or hypogonadism/genital abnormalities, which are frequently observed in BBS.[21] Based on the main organ involvement, JBTS can be classified into eight subgroups: classic JBTS, JBTS with ocular defect, JBTS with renal defect, JBTS with oculorenal defects, JBTS with hepatic defect, JBTS with oral–facial–digital defects, JBTS with acrocallosal features, and JBTS with JATD.[9,13] The combination of the clinical features, MTS, polydactyly, midline cleft/notch of the upper lip suggests that the *IFT74*-associated patients represent the oral–facial–digital subgroup of JBTS with or without optic nerve hypoplasia. Given the substantial phenotypic variability and genetic heterogeneity of JBTS, it is remarkable that all four patients present with similar clinical features and have identical genetic causes (a truncated variant in *IFT74* together with a p.Q179E substitution), thus establishing an genotype–phenotype correlation of JBTS.

The IFT-B subcomplex is responsible for anterograde transport in cilia, and null alleles of most IFT-B genes usually cause a complete loss of cilia.[3,4] Consistent with the incompatibility of mammalian development without cilia, null variants in both alleles of IFT-B genes have not been identified in human cases, indicating a critical role of IFT-B in health.[3] Previously described JBTS-associated proteins localize at key parts of cilia to regulate ciliary compositions and signaling, but the function of IFT, a major module of cilia, in JBTS was largely unknown. In this study, we show the genetic link between JBTS and an IFT-B core subunit. Consistent with reported variants in IFT genes, the affected individuals harbor a conserved missense allele in *trans* and with another truncated allele. Our mechanistic investigations indicate that pathogenic variants in *IFT74* cause defects in ciliary length, ciliogenesis, ciliary components (ARL13B and INPP5E), and Hh signaling (GPR161 accumulation in cilia and aberrant transcription of targeted genes).

Ciliopathies encompass a plethora of heterogeneously syndromic and nonsyndromic genetic disorders that reflect the versatile roles of cilia in motility, sensory, and signaling functions.[1–3] How specific variants in the same ciliary protein generate a spectrum of discrete pleiotropic clinical features in ciliopathies is puzzling. We found that, in contrast to the p.Q179E variant, the BBS variant (Δ561–600-IFT74) almost completely lost its binding ability with IFT27 (BBS19). This in vitro study demonstrated that distinct IFT74 variants caused different biochemical consequences in JBTS and BBS.

Conclusion

In this study, we have identified *IFT74* as a JBTS-related gene, and the affected individuals with *IFT74* variants represent an oral–facial–digital subtype of JBTS (Fig. S8). Our work links the IFT-B core complex with JBTS and provides cellular and biochemical insights. This finding expands the genetic spectrum of ciliopathies caused by IFT genes and improves the molecular diagnosis of JBTS. Given the presumable cooperativity of IFT components, it will be of interest to screen other genes encoding IFT proteins in uncharacterized JBTS patients.

DATA AVAILABILITY

The DNA, RNA, proteins, reagents, and the data in this study are available upon request.

Received: 8 October 2020; Accepted: 13 January 2021;
Published online: 2 February 2021

REFERENCES

1. Fliegauf, M., Benzing, T. & Omran, H. When cilia go bad: cilia defects and ciliopathies. *Nat. Rev. Mol. Cell. Biol.* **8**, 880–893 (2007).
2. Reiter, J. F. & Leroux, M. R. Genes and molecular pathways underpinning ciliopathies. *Nat. Rev. Mol. Cell. Biol.* **18**, 533–547 (2017).
3. Pazour, G. J., Quarmby, L., Smith, A. O., Desai, P. B. & Schmidts, M. Cilia in cystic kidney and other diseases. *Cell. Signal.* **69**, 109519 (2020).
4. Rosenbaum, J. L. & Witman, G. B. Intraflagellar transport. *Nat. Rev. Mol. Cell. Biol.* **3**, 813–825 (2002).
5. Hildebrandt, F., Benzing, T. & Katsanis, N. Ciliopathies. *N. Engl. J. Med.* **364**, 1533–1543 (2011).
6. Bachmann-Gagescu, R. et al. Healthcare recommendations for Joubert syndrome. *Am. J. Med. Genet. A* **182**, 229–249 (2020).
7. Sattar, S. & Gleeson, J. G. The ciliopathies in neuronal development: a clinical approach to investigation of Joubert syndrome and Joubert syndrome-related disorders. *Dev. Med. Child Neurol.* **53**, 793–798 (2011).
8. Bachmann-Gagescu, R. et al. Joubert syndrome: a model for untangling recessive disorders with extreme genetic heterogeneity. *J. Med. Genet.* **52**, 514–522 (2015).
9. Brancati, F., Dallapiccola, B. & Valente, E. M. Joubert syndrome and related disorders. *Orphanet J. Rare Dis.* **5**, 20 (2010).
10. Garcia-Gonzalo, F. R. et al. A transition zone complex regulates mammalian ciliogenesis and ciliary membrane composition. *Nat. Genet.* **43**, 776–784 (2011).
11. Sang, L. et al. Mapping the NPHP-JBTS-MKS protein network reveals ciliopathy disease genes and pathways. *Cell.* **145**, 513–528 (2011).
12. Vilboux, T. et al. Molecular genetic findings and clinical correlations in 100 patients with Joubert syndrome and related disorders prospectively evaluated at a single center. *Genet. Med.* **19**, 875–882 (2017).
13. Parisi, M. A. The molecular genetics of Joubert syndrome and related ciliopathies: the challenges of genetic and phenotypic heterogeneity. Transl Sci. *Rare Dis.* **4**, 25–49 (2019).
14. Halbritter, J. et al. Defects in the IFT-B component IFT172 cause Jeune and Mainzer–Saldino syndromes in humans. *Am. J. Hum. Genet.* **93**, 915–925 (2013).
15. Richards, S. et al. Standards and guidelines for the interpretation of sequence variants: a joint consensus recommendation of the American College of Medical Genetics and Genomics and the Association for Molecular Pathology. *Genet. Med.* **17**, 405–424 (2015).
16. Lek, M. et al. Analysis of protein-coding genetic variation in 60,706 humans. *Nature* **536**, 285–291 (2016).
17. Brooks, B. P. et al. Joubert syndrome: ophthalmological findings in correlation with genotype and hepatorenal disease in 99 patients prospectively evaluated at a single center. *Ophthalmology* **125**, 1937–1952 (2018).
18. Lucker, B. F. et al. Characterization of the intraflagellar transport complex B core: direct interaction of the IFT81 and IFT74/72 subunits. *J. Biol. Chem.* **280**, 27688–27696 (2005).
19. Bhogaraju, S. et al. Molecular basis of tubulin transport within the cilium by IFT74 and IFT81. *Science* **341**, 1009–1012 (2013).
20. Brown, J. M., Cochran, D. A., Craige, B., Kubo, T. & Witman, G. B. Assembly of IFT trains at the ciliary base depends on IFT74. *Curr. Biol.* **25**, 1583–1593 (2015).
21. Lindstrand, A. et al. Copy-number variation contributes to the mutational load of Bardet–Biedl syndrome. *Am. J. Hum. Genet.* **99**, 318–336 (2016).
22. Kleinendorst, L. et al. Second case of Bardet–Biedl syndrome caused by biallelic variants in IFT74. *Eur. J. Hum. Genet.* **28**, 943–946 (2020).
23. Zhang, X. et al. Cilia-driven cerebrospinal fluid flow directs expression of urotensin neuropeptides to straighten the vertebrate body axis. *Nat. Genet.* **50**, 1666–1673 (2018).
24. Shi, L. et al. Intraflagellar transport protein 74 is essential for spermatogenesis and male fertility in micedagger. *Biol. Reprod.* **101**, 188–199 (2019).
25. Eguether, T. et al. IFT27 links the BBSome to IFT for maintenance of the ciliary signaling compartment. *Dev. Cell.* **31**, 279–290 (2014).
26. Baala, L. et al. The Meckel-Gruber syndrome gene, MKS3, is mutated in Joubert syndrome. *Am. J. Hum. Genet.* **80**, 186–194 (2007).
27. Yang, T. T. et al. Superresolution pattern recognition reveals the architectural map of the ciliary transition zone. *Sci. Rep.* **5**, 14096 (2015).
28. Coene, K. L. et al. OFD1 is mutated in X-linked Joubert syndrome and interacts with LCA5-encoded lebercilin. *Am. J. Hum. Genet.* **85**, 465–481 (2009).

29. Cantagrel, V. et al. Mutations in the cilia gene ARL13B lead to the classical form of Joubert syndrome. *Am. J. Hum. Genet.* **83**, 170–179 (2008).
30. Cevik, S. et al. Active transport and diffusion barriers restrict Joubert syndrome-associated ARL13B/ARL-13 to an Inv-like ciliary membrane subdomain. *PLoS Genet*. **9**, e1003977 (2013).
31. Liem, K. F. Jr. et al. The IFT-A complex regulates Shh signaling through cilia structure and membrane protein trafficking. *J. Cell. Biol.* **197**, 789–800 (2012).
32. Nozaki, S. et al. Regulation of ciliary retrograde protein trafficking by Joubert syndrome proteins ARL13B and INPP5E. *J. Cell. Sci.* **130**, 563–576 (2016).
33. Humbert, M. C. et al. ARL13B, PDE6D, and CEP164 form a functional network for INPP5E ciliary targeting. *Proc. Natl. Acad. Sci. U. S. A.* **109**, 19691–19696 (2012).
34. Garcia-Gonzalo, F. R. et al. Phosphoinositides regulate ciliary protein trafficking to modulate hedgehog signaling. *Dev. Cell.* **34**, 400–409 (2015).
35. Dawe, H. R. et al. The Meckel-Gruber syndrome proteins MKS1 and meckelin interact and are required for primary cilium formation. *Hum. Mol. Genet.* **16**, 173–186 (2007).
36. Scholey, J. M. & Anderson, K. V. Intraflagellar transport and cilium-based signaling. *Cell.* **125**, 439–442 (2006).
37. Dafinger, C. et al. Mutations in KIF7 link Joubert syndrome with Sonic Hedgehog signaling and microtubule dynamics. *J. Clin. Invest*. **121**, 2662–2667 (2011).
38. Shimada, H. et al. In vitro modeling using ciliopathy-patient-derived cells reveals distinct cilia dysfunctions caused by CEP290 mutations. *Cell. Rep.* **20**, 384–396 (2017).
39. Mukhopadhyay, S. et al. The ciliary G-protein-coupled receptor Gpr161 negatively regulates the Sonic hedgehog pathway via cAMP signaling. *Cell*. **152**, 210–223 (2013).
40. Mukhopadhyay, S. et al. TULP3 bridges the IFT-A complex and membrane phosphoinositides to promote trafficking of G protein-coupled receptors into primary cilia. *Genes Dev*. **24**, 2180–2193 (2010).

ACKNOWLEDGEMENTS

We thank the patients and their parents for their participation in this research and their permission for this publication. This work was supported by National Key Research and Development Program of China (2016YFC1000307) to X.M., National Natural Science Foundation of China (91954123, 31972887) to M.C., Clinical research projects of Shanghai Municipal Health Commission (20194Y0133) to M.C., National Nature Science Foundation of China (81873687) to R.S., CAMS Innovation Fund for Medical Sciences (CIFMS 2016-I2M-1-002) to R.S., Beijing Natural Science Foundation (7152116) to R.S., the Non-profit Central Research Institute Fund of National Research Institute for Family Planning (2020GJZ05) to M.L., National Natural Science Foundation of China (31701172) to D.M., Natural Science Foundation of Tianjin (18JCQNJC09900) to D.M., Qingdao National Laboratory for Marine Science and Technology (No.MS2019NO02) to C.Z., and the National Natural Science Foundation of China (31991194) to C.Z.

AUTHOR CONTRIBUTIONS

M.C., X.M., C.Z., R.S., and M.L. conceived the concept and supervised the studies. Y.Z., G.L., X.W., and L.C. collected the blood samples and clinical data of the patients. M.L., Z.C., Y.S., C.L., R.C., and H.G. performed the human genetic study. R.S., M.L., T.Z., H.L., and X.Z. acquired, analyzed, and interpreted the clinical data. R.S., T.Z., and S.W. conducted skin biopsies and primary cell culture. Z.L., D.M., R.H., M.H., and H.J. performed the biochemical analysis, cell biology, imaging, and data analysis. M.J. performed the animal experiments. M.L., Z.L., T.Z., and M.J. contributed equally to the data and thus are credited as co–first authors. M.C., X.M., C.Z., and R.S. wrote the manuscript with input from all authors.

ETHICS DECLARATION

This study was performed in accordance with the contents of the Declaration of Helsinki and was approved by the Institutional Review Board of the National Research Institute for Family Planning (NRIFP) and Peking Union Medical College Hospital (PUMCH). All patient information, photos, and samples from the probands and/or their parents/sibling were collected after receiving written consent. All zebrafish experiments were conducted according to standard animal guidelines and were approved by the Institutional Animal Care Committee of Ocean University of China.

COMPETING INTERESTS

The authors declare no competing interests.

ADDITIONAL INFORMATION

Supplementary information The online version contains supplementary material available at https://doi.org/10.1038/s41436-021-01106-z.

Correspondence and requests for materials should be addressed to R.S., C.Z., X.M. or M.C.

Reprints and permission information is available at http://www.nature.com/reprints

Publisher's note Springer Nature remains neutral with regard to jurisdictional claims in published maps and institutional affiliations.